



## Statistical relationships between cosmic radio noise absorption and ionospheric electrical conductances in the auroral zone

A. Senior,<sup>1</sup> A. J. Kavanagh,<sup>1</sup> M. J. Kosch,<sup>1</sup> and F. Honary<sup>1</sup>

Received 2 May 2007; revised 3 July 2007; accepted 20 August 2007; published 10 November 2007.

[1] Statistical models expressing the Hall and Pedersen conductances and their ratio as functions of cosmic noise absorption (CNA) are derived for five intervals of magnetic local time (MLT). The models are based on simultaneous measurements of electron densities from the European Incoherent Scatter UHF radar at Tromsø (69.6°N, 19.2°E) and absorption from the imaging riometer at Kilpisjärvi (69.1°N, 20.8°E). The Hall conductance and the conductance ratio are found to be rather strongly related to CNA, whereas the Pedersen conductance is less so. The Hall conductance-CNA relationship is strongly dependent on MLT. These results are interpreted as being the consequence of the particular sensitivity of CNA to the typical energy of electron precipitation, the latter changing as a function of MLT as the electrons drift around the Earth. The models are compared to a previous study which did not use simultaneous measurements or take into account the MLT dependence. There is a significant difference between that study and the results presented here.

**Citation:** Senior, A., A. J. Kavanagh, M. J. Kosch, and F. Honary (2007), Statistical relationships between cosmic radio noise absorption and ionospheric electrical conductances in the auroral zone, *J. Geophys. Res.*, 112, A11301, doi:10.1029/2007JA012519.

### 1. Introduction

[2] The electrical conductivity of the ionosphere is fundamentally important to the study of magnetosphere-ionosphere coupling and therefore to that of energy flow in the solar-terrestrial system. The conductivity arises in the lower ionosphere (*D* and *E* regions) where the increased collision frequency primarily between ions and neutrals permits differential electron-ion drift under an imposed electric field in the presence of the geomagnetic field. The ionization in these regions comes from two main sources: solar illumination at ultraviolet and X-ray wavelengths and the impact of energetic electrons (and ions) from the magnetosphere. The latter is especially important at high latitudes where magnetosphere-ionosphere coupling currents flow.

[3] The conductivity is usually determined indirectly as the relevant regions are difficult to access for in situ measurements. If the electron density is known, then the conductivity can be calculated from theory using model values for the ion-neutral collision frequencies. Electron density may be determined from instruments such as ionosondes or incoherent scatter radars, but these suffer from limitations such as the inability to survey large areas either at all or on a short timescale compared to the timescale on which the ionosphere changes significantly. For large-scale studies the inversion of optical and X-ray

measurements from space permits reconstruction of precipitating particle fluxes and hence electron densities and conductivities [Aksnes *et al.*, 2006]. On the medium scale, similar techniques can be applied to ground-based optical data [Kosch *et al.*, 1998, 2001; Janhunen, 2001; Partamies *et al.*, 2004; Ashrafi *et al.*, 2005]. However, this approach suffers from the severe limitation of requiring clear skies.

[4] The imaging riometer [Detrick and Rosenberg, 1990] is a ground-based device which makes medium-scale measurements of the ionospheric absorption of cosmic radio noise at very high frequencies (~30 MHz). This absorption is a good indicator of *D* and *E* region ionization because of energetic electron precipitation [Hargreaves, 1969]. Absorption is determined by comparing the cosmic noise power received to the level expected in the absence of reductions due to precipitation enhancing the lower ionosphere (a “quiet day”). As a result, the ionization due to solar illumination is not detected. Since the electron precipitation is also responsible for enhancing the conductivity, it is natural to seek relationships between cosmic noise absorption (CNA) and conductivity once the solar ionization contribution to the latter has been taken into account. Furthermore, riometers unlike ground-based photometers and imagers, are able to operate regardless of cloud cover and daylight and can perform continuous monitoring.

[5] Walker and Bhatnagar [1989] derived empirical relationships between CNA and conductivities using statistical electron density profiles determined for several values of CNA by Collis *et al.* [1984]. In this work the relationships between CNA and conductivity are investigated using simultaneous measurements with a common ionospheric volume from an imaging riometer and an incoherent scatter

<sup>1</sup>Department of Communication Systems, Lancaster University, Lancaster, UK.

radar. The latter is used to determine the conductivity from the measured profiles of electron density. The results differ significantly from those of *Walker and Bhatnagar* [1989].

## 2. Theory

[6] The ionospheric absorption of cosmic radio noise at the riometer angular frequency  $\omega_R$  is given by the formulae [Hargreaves, 1969]

$$A = \int N_e a dz \quad (1)$$

$$a = \frac{4.6 \times 10^{-5} \nu}{\nu^2 + (\omega_R \pm \omega_e)^2}, \quad (2)$$

where  $A$  is in dB,  $N_e$  is the electron number density in  $\text{m}^{-3}$ ,  $\omega_e$  is the electron angular gyrofrequency,  $\nu$  is the electron collision frequency, and  $a$  is known as the “specific absorption” and has units of  $\text{dB m}^2$ , that is, absorption per unit electron density per unit altitude. The positive sign in the denominator of (2) corresponds to a O-mode wave and the negative sign to a X-mode wave, which riometers are frequently built to receive.

[7] The ionospheric Pedersen and Hall conductances  $\Sigma_{H,P}$  are the height-integrated (along the magnetic field) Pedersen and Hall conductivities  $\sigma_{H,P}$ . The conductances are used since the conductivity parallel to the magnetic field is very high, and so the conductivity layers at different altitudes are effectively connected in parallel. Conductivity  $\sigma$  is related to mobility  $\mu$  by  $\sigma = N_e e \mu$ , where  $e$  is the electronic charge. The conductances are then

$$\Sigma_{H,P} = e \int N_e \mu_{H,P} dz, \quad (3)$$

where the mobilities are [Davies and Lester, 1999]

$$\mu_H = \frac{1}{B} \left( \frac{\omega_e^2}{\nu_{en}^2 + \omega_e^2} - \sum_j P_j \frac{\omega_j^2}{\nu_{jn}^2 + \omega_j^2} \right) \quad (4)$$

$$\mu_P = \frac{1}{B} \left( \frac{\omega_e \nu_{en}}{\nu_{en}^2 + \omega_e^2} + \sum_j P_j \frac{\omega_j \nu_{jn}}{\nu_{jn}^2 + \omega_j^2} \right), \quad (5)$$

where  $\mu_H$  and  $\mu_P$  are the Hall and Pedersen mobilities, respectively;  $j$  refers to an ion species;  $\omega_j$  is the gyrofrequency of ion species  $j$ ;  $\nu_{jn}$  is the ion-neutral collision frequency for ion species  $j$ ;  $P_j$  is the relative density of ion species  $j$ ; and  $B(z)$  is the geomagnetic flux density.

[8] There is an obvious similarity between (1) and (3) in that both take the form of a convolution of the electron density profile with a profile of some other parameter. Neglecting transport, the equilibrium electron density is given by  $N_e = \sqrt{(q/\alpha)}$ , where  $q$  is the ionization production rate and  $\alpha$  is the effective recombination coefficient. In section 1 it was explained that CNA does not include the ionization contribution from solar radiation, so only the

contribution from particle impact is considered. Since the conductances certainly do include a contribution from solar ionization, this contribution must be subtracted before comparing them with CNA. This procedure is described in section 3.2. Now, neglecting solar radiation,  $q$  is proportional to the rate of energy deposition by precipitating particles at each altitude [Rees, 1963]. It follows that the height-integrated production rate is proportional to the integral energy flux of the precipitation  $\Phi_E$ . Therefore, for a given  $\Phi_E$  the height profile of  $q$  is determined by the shape of the precipitating particle flux-energy spectrum. Note that with this definition of “shape” two Maxwellian spectra with different characteristic energies would have different “shapes.”

[9] Now the integral number flux  $\Phi$  is given by  $\Phi = \Phi_E \bar{E}$ , where  $\bar{E}$  is the mean energy, a function of the shape of the spectrum. Thus it follows that  $q \propto \Phi_E = \bar{E} \Phi$ . Recalling that the “constant” of proportionality is a function of the spectrum shape and noting that to first order,  $\bar{E}$  is a measure of this shape  $q = f(\bar{E}) \Phi$ , where  $f$  is some arbitrary spectrum-shape-dependent function. Thus we have  $N_e = f(\bar{E}) \Phi^{0.5}$  by the equilibrium condition (where  $f$  is some other arbitrary function).

[10] Since absorption and conductance are convolutions involving the electron density profile, it follows that they all take the form  $P = f(\bar{E}) \Phi^{0.5}$ , that is, they are all proportional to the square root of the integral number flux by some energy-dependent factor, which differs from parameter to parameter. It also follows that ratios of the parameters, in particular,  $\Sigma_H/\Sigma_P$  are indicators of the energy. An important consequence of this result is that although the conductances and CNA scale in the same way with changes in integral flux, they respond differently to changes in the spectrum shape (“energy”). This corresponds with intuition given that the conductances and CNA are associated with different altitude intervals ( $\Sigma_P \sim 110\text{--}130$  km,  $\Sigma_H \sim 80\text{--}110$  km, CNA  $< 100$  km) and thus with different parts of the flux-energy spectrum ( $\Sigma_P \sim 2\text{--}10$  keV,  $\Sigma_H \sim 5\text{--}50$  keV, CNA  $> 20$  keV). Thus it is clear that there will not be a one-one relationship between CNA and conductance, but rather it will be of a statistical nature depending on changes in the spectrum shape.

## 3. Experimental Data

### 3.1. Instrumentation

[11] In this study, CNA measurements are taken from the imaging riometer for ionospheric studies (IRIS) at Kilpisjärvi, Finland (69.05°N, 20.79°E) [Browne et al., 1995]. A statistical study of IRIS measurements was given by *Kavanagh et al.* [2004]. The conductances are calculated from measurements taken using the European Incoherent Scatter (EISCAT) UHF radar [Rishbeth and van Eyken, 1993] located near Tromsø, Norway (69.58°N, 19.23°E). The radar data are taken from Common Program One (CP-1) operations where the beam is directed along the magnetic field. *Davies and Lester* [1999] presented statistics of conductances determined from similar measurements. The riometer beam (referred to as beam 16), which intersects the radar beam at an altitude of 90 km, was chosen for the absorption measurements. The riometer operates at a frequency of 38.2 MHz. Both the radar and riometer measurements were

**Table 1.** List of the EISCAT CP-1 Data Sets Used in This Study<sup>a</sup>

Date	Start, UT	End, UT
5 Oct 2002	1041	2359
6 Oct 2002	0000	2359
7 Oct 2002	0000	2359
8 Oct 2002	0000	2359
9 Oct 2002	0000	2359
10 Oct 2002	0000	2359
11 Oct 2002	0000	2359
12 Oct 2002	0000	1231
23 Sep 2003	0000	2359
24 Sep 2003	0000	2359
25 Sep 2003	0000	2359
26 Sep 2003	0000	1500
10 Mar 2004	0747	2359
11 Mar 2004	0000	2359
12 Mar 2004	0000	1359
1 Jun 2004	0700	2359
2 Jun 2004	0000	2359
3 Jun 2004	0000	2359
4 Jun 2004	0000	1559
7 Mar 2006	0000	2359
8 Mar 2006	0000	2359
24 Mar 2006	0000	2259
28 Mar 2006	0000	2359
29 Mar 2006	0000	2359
30 Mar 2006	0000	2359
31 Mar 2006	0000	2359
4 Apr 2006	0000	2359
5 Apr 2006	0000	2359
6 Apr 2006	0000	1305

<sup>a</sup>Some data sets contain gaps which are not indicated here.

integrated over 60 s intervals. The riometer has a basic time resolution of 1 s, and the radar has a basic time resolution of 5 s. These shorter integrations would be more appropriate to the rapidly-changing auroral conditions, but the measurement variance for the radar data would become very large. Ideally, the CNA and conductance should be compared when both are steady state to avoid inconsistencies due to their

differing response times to precipitation (the recombination time). This was investigated by using 5 s resolution CNA data to eliminate 60 s integrations where the CNA was highly variable during the integration time, but removing these integrations was not found to greatly influence the results.

### 3.2. Data Selection and Preparation

[12] Data from 29 days between 2002 and 2006 on which the UHF radar ran the CP-1 mode were selected for analysis (Table 1). The days were selected to give as close to 24-h coverage as possible in both the radar and riometer data. Data from 9–13 November 2004 were not used because of a solar proton event. Energetic proton precipitation enhances CNA but produces ionization at altitudes too low to significantly affect the conductances. The distribution of data points by magnetic local time (MLT) is shown in Figure 1.  $MLT \approx UT + 2.5$  h at Tromsø and this approximate relationship is used throughout this study. The reduced occurrence in the 0400–0800 and 1700–2100 MLT intervals is due to the omission of periods where the riometer measurement was affected by scintillation in the October 2002 and March/April 2006 data sets, respectively (see later). Consequently, these time sectors are biased toward the March/April 2006 and October 2002 data sets, respectively.

[13] The UHF radar spectra were analysed at 60-s resolution using the Grand Unified Incoherent Scatter Design and Analysis Package (GUISDAP) [Lehtinen and Huuskonen, 1996]. As fitting the spectrum is an under-determined problem, certain standard assumptions are made about some parameters. The ion composition is assumed rather than fitted at all heights. Above 107 km the electron/ion temperature ratio is fitted and the ion-neutral collision frequency held constant. Below 107 km the reverse situation applies with the electron/ion temperature ratio taken equal to  $\sim 1.1$ . The electron density, ion temperature, and line-of-sight ion drift velocity are fitted at all heights.

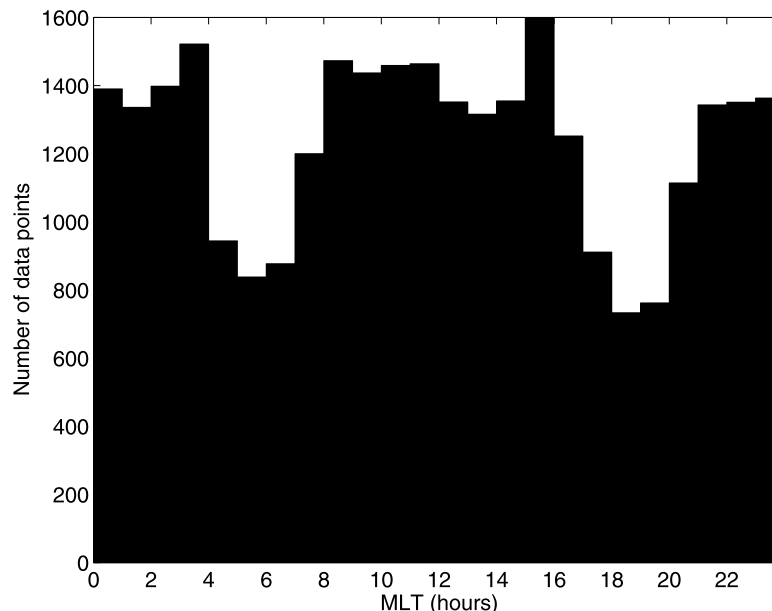


**Figure 1.** Distribution of data used in this study by magnetic local time.

[14] Since the analysis of the incoherent scatter ion line only determines the electron density up to a scale factor, the electron densities were calibrated by comparing the peak  $F$  region density in each profile against the corresponding  $f_oF_2$  value from the EISCAT dynasonde ionospheric sounder. This calibration is valid for the whole altitude range. The resulting plasma parameters were filtered to exclude obviously non-physical fits (e.g., negative temperatures, electron densities or ion-neutral collision frequencies, or electron densities exceeding  $10^{13} \text{ m}^{-3}$  which probably indicate backscatter from space debris or satellites).

[15] For each altitude profile the Pedersen and Hall conductivities were computed for each altitude gate using (3–5). The ion-neutral collision frequencies were calculated using the formulae of *Schunk and Walker* [1973], and the electron-neutral collision frequency was calculated using the formula of *Schunk and Nagy* [1978]. The MSISE-90 and IRI-2001 models were run for each time point to give the neutral densities and ion composition. The ion and electron temperatures were taken from the radar data. The conductivities were filtered to remove nonphysical negative values which can result from unrealistically high ion or electron temperatures from the radar analysis being used in the collision frequency formulae. Altitude profiles having fewer than 50% of range gates containing valid data were excluded from further analysis. This reduces the number of very noisy estimates of the conductances but introduces some slight bias since profiles having very low electron densities (and thus poor radar signal-to-noise ratios) are likely to be lost. The conductivities were then integrated over the altitude range 85–200 km, according to (3) to give the conductances.

[16] Since the riometer only measures the CNA because of enhanced particle precipitation, the solar ionization contribution to the conductances was subtracted. In principle the ionization production rate due to solar ionization should be subtracted from the total production rate. In equilibrium and under the assumption of an  $\alpha$ -type recombination model the production rate is  $q = \alpha N_e^2$ . Since conductance is  $\Sigma \propto N_e$ , it follows that the subtraction becomes  $\Sigma^* = \sqrt{\Sigma^2 - \Sigma_S^2}$ , where  $\Sigma$  is the total conductance,  $\Sigma^*$  is the conductance due to particle precipitation, and  $\Sigma_S$  is the conductance due to solar ionization (strictly, since conductances are height-integrated, one should work with conductivities). In this study,  $\Sigma_S$  comes from the empirical models of *Brekke and Hall* [1988] which are functions of solar zenith angle. However, *Brekke et al.* [1989] pointed out that the form of these models is not consistent with the simple picture of  $\alpha$ -type recombination and hence preferred simply to subtract the conductances directly, that is,  $\Sigma^* = \Sigma - \Sigma_S$ . This direct subtraction is adopted in this study.

[17] At a final stage of filtering, values of the conductances and their ratio lying more than 4 standard deviations from the mean of each daily data set were excluded to avoid “wild” values from distorting the statistics. This filtering was intended to remove remaining anomalous data points resulting from technical problems with the radar and reflections from satellites which were not removed in the earlier processing. Inevitably, there is a risk that some valid data were removed just as there is that some invalid data were not. Additionally, for the conductance ratio only, points

having estimated standard errors greater than 0.5 were rejected. This mitigates the problem described by *Brekke and Hall* [1988] where subtracting the solar contribution to the conductance causes the estimate of the ratio to become noisy, for example, if the corrected  $\Sigma_P$  is close to zero.

[18] The CNA data from beam 16 of IRIS were averaged to 60-second resolution. Periods where ionospheric scintillation was present were removed. For each day listed in Table 1 the data were shifted by an offset to compensate for inaccuracy in the estimated quiet day absorption level. Just under half of these offsets were zero, but one was as large as 0.25 dB (23 September 2003). The offsets were obtained by inspection of daily line plots of absorption. This method obviously does not allow for an offset which varies during a given day. Finally, CNA values less than  $-0.5$  dB, which are likely to be the result of interference, were excluded.

### 3.3. Results

[19] Figure 2 shows occurrence plots of the Hall conductance versus CNA, as a function of magnetic local time interval. The intervals were chosen by inspecting scatter plots of the data over shorter periods of MLT in order to determine the intervals over which the distribution was reasonably constant. Four main populations of data points were found, corresponding to the intervals 1900–0400, 0400–1000, 1000–1500, and 1500–1900 MLT. The 1900–0400 and 1000–1500 MLT populations are clearly quite different. During the intervening interval 0400–1000 MLT the distribution gradually alters from that of 1900–0400 to that of 1000–1500 MLT and this interval (0400–1000 MLT) has been subdivided into three 2-h intervals in Figure 2. In the 1500–1900 MLT interval, there is very little enhancement of Hall conductance or CNA.

[20] This classification has been adopted for the data analysis since the four main populations correspond well with what might be expected from the physical processes underlying the particle precipitation. The 1900–0400 MLT interval coincides with the interval where substorms occur, injecting particles directly on to the field lines within the instruments’ field of view [*Baker et al.*, 1981; *Thomsen et al.*, 2001]. In the interval 1000–1500 MLT the precipitation comes mainly from energetic electrons gradient-curvature drifting eastward from substorm injection at earlier MLTs [*Jelly and Brice*, 1967; *Roederer*, 1967; *Hargreaves*, 1968; *Hargreaves and Devlin*, 1990]. The intervening interval 0400–1000 MLT then contains a mixture of precipitation from local substorms and from drifting electrons. Satellite observations [*Collis et al.*, 1984; *Hardy et al.*, 1985] have shown that the precipitation spectrum becomes progressively harder with increasing MLT, at least until about 0900 MLT, although bremsstrahlung X-ray measurements [*Bewersdorff et al.*, 1966; *Kodama et al.*, 1995] suggest that the hardening continues toward dusk. In the final interval 1500–1900 MLT, very little enhancement of CNA or the conductances occurs. This interval has long been known to be a minimum in precipitation as detected by CNA [*Brown*, 1966; *Hargreaves*, 1969].

### 3.4. Measurement Uncertainties

[21] There are a number of factors which contribute to uncertainties in the measurements. Considering the riometer data, the random error in the 60 s integrated data is small,

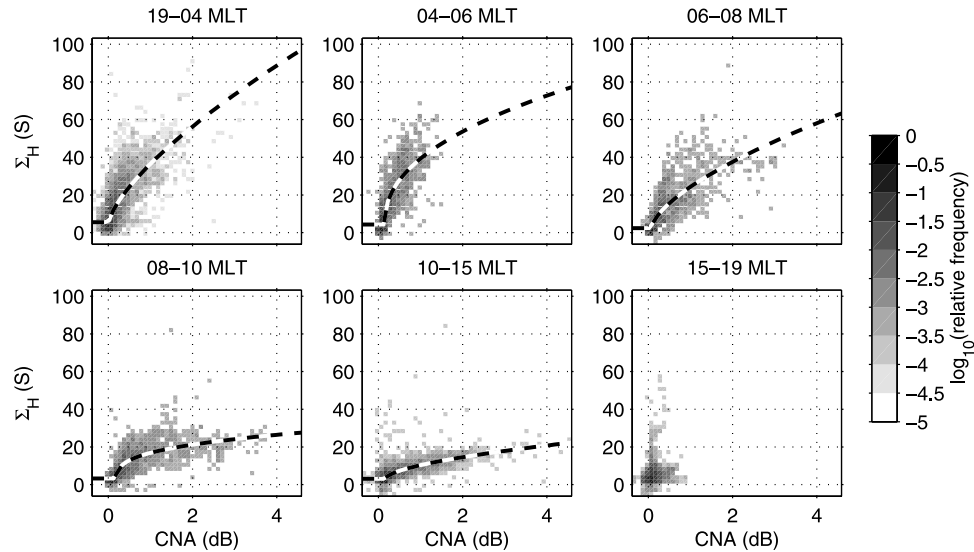


**Figure 2.** Occurrence plots of Hall conductance versus CNA for six intervals of magnetic local time. The intensity of shading represents the proportion of the total number of points (the relative frequency) in each bin. The dashed curves are the means of the fitted models. The MLT intervals are indicated.

having a standard deviation of about 0.01 dB, rising to 0.1 dB during very rapidly varying absorption or scintillation, although periods of scintillation have been excluded here. This is small compared to the range of absorption values observed. On the other hand, systematic errors result from inaccurate estimation of the quiet day level, that is, the cosmic noise power received in the absence of precipitation enhancing the *D* region electron density. These systematic errors are on the order of 0.2 dB. As described earlier, the CNA data have been adjusted to reduce this error, but it is difficult to completely eliminate it. An error of 0.2 dB is rather large compared to the range of absorption measured.

[22] In the case of the radar data the main source of uncertainty is the random error associated ultimately with the signal-to-noise ratio of the plasma spectrum measurement. The uncertainties of the plasma parameters are estimated by the analysis software. The parameters used in calculating the conductances are the electron density and the electron and ion temperatures. The temperatures affect the result in a relatively complicated manner, but the effect of uncertainty in the electron density is easier to estimate and on the basis of this 94% (77%) of the Hall conductances and 98% (90%) of the Pedersen conductances have errors less than 10% (5%).

[23] Systematic errors can arise because of the failure of the assumptions made in the radar analysis and calculation of the conductances. For example, if the model ion composition does not reflect reality, the temperatures obtained from the radar analysis will be incorrect, as will the collision frequencies used in calculating the conductivities. Such a situation can arise, for example, during ion frictional heating because of strong electric fields, leading to an increase in the proportion of molecular ions in the lower *F* region. In the *E* region the same electric fields can excite the Farley-Buneman instability leading to electron heating, violating the assumption that the electron/ion temperature ratio is fixed below 107 km [Davies and Robinson, 1997]. This

same phenomenon has also been found to affect CNA [Stauning, 1984].

[24] An additional source of error results from the different fields of view of the riometer and radar. The radar beam has a width of approximately  $0.6^\circ$  and is directed at a zenith angle of  $13^\circ$  through the ionosphere. On the other hand, the riometer beam chosen has a width of about  $12^\circ$  and passes more obliquely through the ionosphere (zenith angle of  $33^\circ$ ). The two instruments thus integrate over very different but intersecting volumes of plasma. The intersection of the beams varies with altitude and therefore with changes in the hardness of the precipitating electron spectrum. Furthermore, if there is small-scale structure in the precipitation (which is certainly observed in optical images of the aurora), then this will also lead to discrepancies between the radar and riometer measurements. Unfortunately, it is almost impossible to estimate this type of error quantitatively.

### 3.5. Statistical Models

[25] In order to have a convenient method by which to make statistical predictions of conductance parameters from CNA, models of the form

$$\mu_Y = \begin{cases} c : A < A_0 \\ m(A - A_0)^p + c : A \geq A_0 \end{cases} \quad (6)$$

have been fitted to the data, where  $A$  is CNA in dB;  $m$ ,  $c$ , and  $p$  are arbitrary nonnegative constants;  $Y$  is the response variable (Hall or Pedersen conductance or the Hall/Pedersen conductance ratio); and  $\mu_Y$  is its mean. As noted earlier, there is no simple theoretical basis on which to expect a particular functional form for the relationship between the conductance parameters and absorption and so the choice of this power law form was based on a number of factors. The data suggest monotonic relationships and when plotted on a log-log scale (not shown) are roughly linear. The constant term  $c$  allows for the possibility that the conductance (or

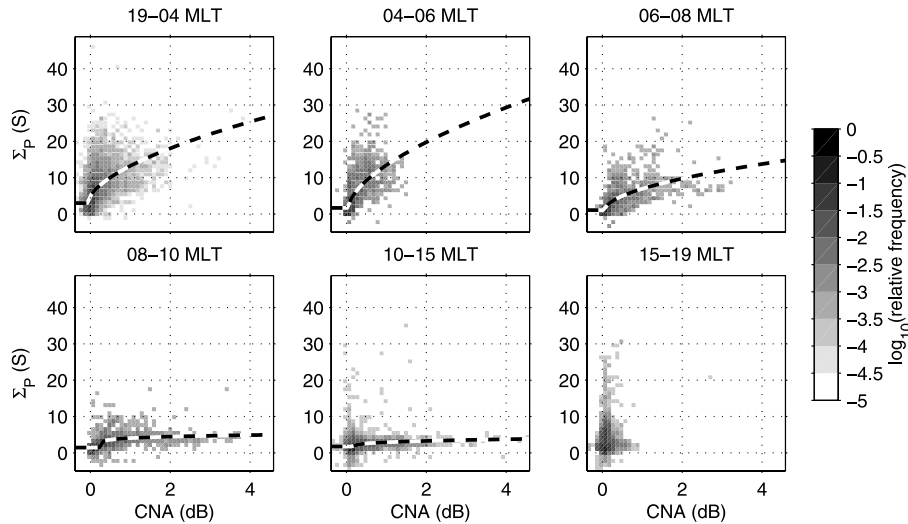


Figure 3. Same as for Figure 2 but for Pedersen conductance versus CNA.

ratio) remains nonzero even when CNA is zero and was again suggested by the data. The constant offset  $A_0$  allows for residual bias in the CNA data due to the type of quiet day level uncertainty described in section 3.4. The model was fitted to the data for each MLT interval (excluding 1500–1900 MLT). The distribution of the response  $Y$  was taken as a gamma distribution since the response can theoretically only take nonnegative values. Further details of the models and the coefficients of the fits are given in Appendix A.

[26] Figures 2–4 show the distribution of all the data points (not just those included in the fits) and the means of the fitted models for each MLT interval. The performance of the fits are measured by the  $R^2$  statistic (see Tables A1–A3 in Appendix A). On the whole, the Pedersen conductance is least well explained by the CNA, the only exception being the 0600–0800 MLT interval when the Hall/Pedersen ratio is worse. This may be due to the cluster of points with  $\Sigma_H/\Sigma_P > 5$  for  $A < 1$  dB. The Hall conductance is most well

explained by CNA in all MLT intervals, although the Hall/Pedersen ratio is only slightly worse except for 0600–0800 MLT (as already discussed above) and also 0400–0600 MLT when the Hall conductance is particularly well explained, possibly a side effect of the smaller number of data points in this interval.

#### 4. Discussion

[27] The results show that Hall conductance is more strongly related to CNA than Pedersen conductance. This result might have been expected on intuitive grounds since the energy ranges of precipitating particles causing the Hall conductance region and the CNA region are closer in altitude than those causing the Pedersen conductance and CNA regions. What is more surprising is the apparent strong relation between the conductance ratio and CNA, since the conductance ratio is dependent purely on the

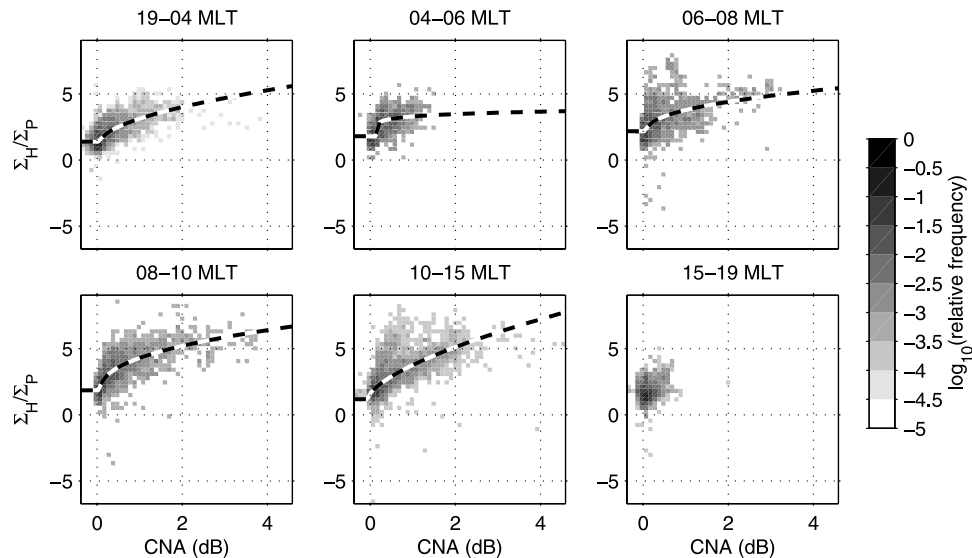
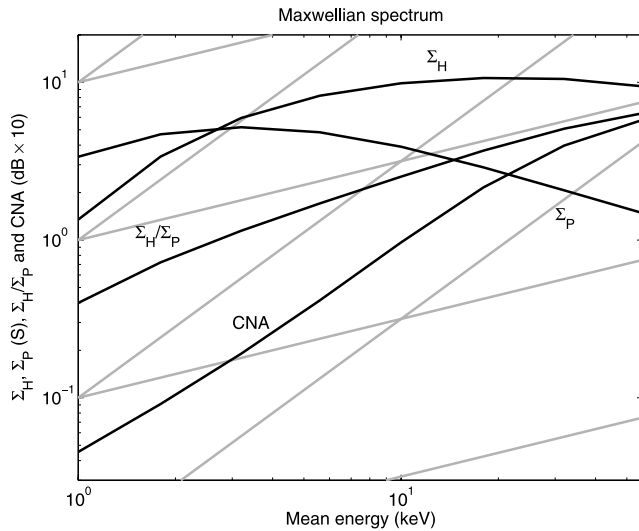


Figure 4. Same as for Figure 2 but for the Hall/Pedersen conductance ratio versus CNA.



**Figure 5.** Calculated values of Pedersen and Hall conductances, their ratio, and CNA for Maxwellian spectra of different mean energies (black curves). The energy flux is  $1 \text{ mW m}^{-2}$  at all energies. The CNA values have been multiplied by 10. The gray curves show how power law functions with indices of 0.5 (shallow slope) and 1.5 (steep slope) would appear on the plot.

energy of the precipitation whereas CNA depends on both the energy and the flux.

[28] Figure 5 shows Pedersen and Hall conductances, their ratio, and CNA computed for Maxwellian electron spectra of different mean energy  $\bar{E}$  for the same energy flux  $\Phi_E = 1 \text{ mW m}^{-2}$ . Fluxes isotropic in pitch angle are assumed. Similar model results for conductances were given by *Vickrey et al.* [1981] and for CNA by *Mori et al.* [2004]. The presentation in terms of constant energy flux follows the previous authors but means that the energy dependence of the parameters is not shown explicitly [*Vickrey et al.*, 1981; *Mori et al.*, 2004]; since  $\Phi_E = \bar{E}\Phi$ , the number flux  $\Phi$  falls in inverse proportion to mean energy  $\bar{E}$ , and since, as discussed earlier, the parameters are proportional to  $\Phi^{0.5}$ , the energy dependence is reduced by a factor of  $\bar{E}^{0.5}$ . The gray curves in Figure 5 have slopes corresponding to power law indices of 0.5 and 1.5. These in turn correspond to explicit power law energy dependencies with indices of 1 and 2, respectively. Thus it is seen that over nearly the whole energy range  $1 < \bar{E} < 50 \text{ keV}$ , CNA is approximately proportional to  $\bar{E}^2$  whereas the energy dependencies of  $\Sigma_P$  and  $\Sigma_H$  are much weaker. It seems likely that the strong association between CNA and  $\Sigma_H/\Sigma_P$  is a result of this strong energy dependence of CNA which dominates its dependence on changes in the number flux of precipitating electrons. From Figure 5,  $\Sigma_H/\Sigma_P$  varies roughly as  $\bar{E}$  over most of the energy range. *Robinson et al.* [1987] found  $\Sigma_H/\Sigma_P \propto \bar{E}^{0.85}$ . Since CNA varies as  $\bar{E}^2$ , it might be expected that  $\Sigma_H/\Sigma_P$  will vary as  $A^{0.5}$  and indeed the power law index in the statistical  $\Sigma_H/\Sigma_P$ -CNA models is not far from 0.5, with the exception of the 0400–0600 MLT interval (Table A3).

[29] A marked contrast between the  $\Sigma_H$ -CNA and  $\Sigma_H/\Sigma_P$ -CNA relationships is their MLT dependence. The MLT

dependence of the former is the basis for the MLT classification used in this study. However, it is clear that the latter has a much weaker if it has any MLT dependence. This can be explained in terms of how the typical energy of precipitating electrons varies with MLT. As remarked on earlier, in the 1900–0400 MLT interval the precipitation is dominated by local substorm activity. Here the electron fluxes tend to be relatively soft. Moving toward later local times, the fluxes become progressively dominated by electrons gradient-curvature drifting eastward (dawnward) from substorm injection and these are observed to become progressively harder with MLT [*Bewersdorff et al.*, 1966; *Hardy et al.*, 1985]. In particular, the satellite measurements presented by *Collis et al.* [1984] support the idea that the energy spectrum hardens in this way and indeed their results agree quite well with the classification into MLT intervals used in this study.

[30] Assuming that the underlying  $\Sigma_H/\Sigma_P$ -CNA relationship is constant (strictly it is a function of the atmospheric response to precipitation), then the observed relationship will not change either, except that there will tend to be more occurrences of high  $\Sigma_H/\Sigma_P$  at later MLTs as the mean energy increases, and Figure 4 supports this. This increase of mean energy can also explain the change in the  $\Sigma_H$ -CNA relationship with MLT. CNA increases much faster with mean energy than  $\Sigma_H$  for a given number flux so that a given CNA tends to correspond to a lower  $\Sigma_H$  at later MLTs.

[31] Relationships between CNA and the Hall and Pedersen conductances were previously derived by *Walker and Bhatnagar* [1989]. They found nearly linear relationships between the Hall and Pedersen conductances and CNA, contrasting with the present power law relationships where the power law index is less than unity. Figure 6 compares the models of *Walker and Bhatnagar* [1989] with those of this work. The *Walker and Bhatnagar* [1989] models were given in terms of CNA at 30 MHz whereas here 38.2 MHz is used. The CNA at 30 MHz was scaled to that at 38.2 MHz assuming it is inversely proportional to the square of the frequency as implied by magnetoionic theory (2). It is clear from Figure 6 that there is a considerable difference between the two sets of models for both the Hall and

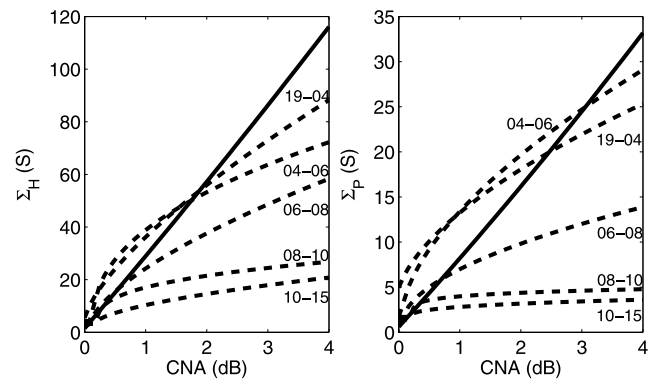


**Figure 6.** Comparison of the conductance-CNA relationships of *Walker and Bhatnagar* [1989] (solid curves) with those of this work (dashed curves) from all magnetic local time sectors ((left) Hall conductance; (right) Pedersen conductance). The CNA is for a frequency of 38.2 MHz.

**Table A1.** Parameters of the Model Fits for Hall Conductance and CNA<sup>a</sup>

MLT	$c$	$m$	$p$	$A_0$	$k$	$n$	$R^2$
1900–0400	5.5 (0.11)	31 (0.52)	0.71 (0.016)	0.014 (0.0044)	4.0 (0.072)	11572	0.59
0400–0600	4.3 (0.20)	37 (1.4)	0.45 (0.048)	0.14 (0.011)	4.1 (0.20)	1778	0.72
0600–0800	2.4 (0.68)	23 (0.55)	0.65 (0.077)	0.076 (0.048)	3.1 (0.35)	2065	0.68
0800–1000	3.2 (0.27)	15 (0.25)	0.34 (0.046)	0.21 (0.027)	2.0 (0.089)	2887	0.66
1000–1500	3.1 (0.14)	8.0 (0.10)	0.59 (0.036)	0.16 (0.023)	1.0 (0.042)	6866	0.57

<sup>a</sup>The parameters of the function (6) are given for each MLT interval. The numbers in parentheses are the approximate errors in the parameters;  $n$  is the number of points included in each fit and  $R^2$  is the fraction of the response variance explained by the fit.

Pedersen conductances. The models match most closely for the 1900–0600 MLT interval, but even there the difference can be a factor of 2 or more. The variation with MLT in the present results is considerable and shows that a single model cannot be used for all MLTs.

[32] The *Walker and Bhatnagar* [1989] models were based on electron density profiles compiled for several different values of CNA by *Collis et al.* [1984]. These profiles were not measured but computed from spacecraft measurements of precipitating electron spectra at geostationary orbit. Furthermore, these calculations included data from all MLTs and are, as the authors pointed out, subject to considerable uncertainty in the effective recombination coefficient [*Collis et al.*, 1984]. As noted earlier in this section and section 3.3, the spacecraft data presented by *Collis et al.* [1984] show that there is significant variation in the typical energy of electron precipitation with MLT and therefore significant variation in the shape of the corresponding electron density profile with MLT. It may be that averaging over these variations resulted in unrealistic electron density profiles and hence unrealistic values for the Pedersen and Hall conductances. In addition, *Walker and Bhatnagar* [1989] had to extrapolate the profiles to higher altitudes to fully cover the conductance region. In contrast, the relationships given here are based on direct comparison of CNA with measured electron density profiles and have been separated by MLT.

[33] *Makarevitch et al.* [2004] presented an interval of simultaneous EISCAT CP-1 and IRIS riometer measurements and established relationships between the Hall conductance and CNA during this interval, which covered the period  $\sim$ 0630–1330 MLT (0400–1100 UT). A simple proportionality,  $\Sigma_H = C_H A$  was used, but they found it necessary to change the constant  $C_H$  from 29.0 for the interval 0630–1030 MLT to 15.5 for the interval 1030–1330 MLT, i.e., in the latter interval, a given CNA corresponded to a smaller Hall conductance. This behavior is qualitatively consistent with the statistical models given here. It so happens in this example that the transition occurred close to the boundary between two of the MLT intervals used here (1000 MLT), but, in general, such

boundaries are not likely to be adhered to. Indeed, it is possible to see from Figure 7 of *Makarevitch et al.* [2004] some sub-intervals when the correlation between  $\Sigma_H$  and CNA is poorer than in others and these are probably due to temporally localized variations in the typical energy of the electron precipitation. Such variations cannot be taken into account by the statistical models and demonstrate a limitation of using them to predict conductances. Indeed, since the models are probability models, it does not follow that if the same absorption is observed at two different times or locations that the conductance must be the same at these two instances but rather that the probability distribution of the conductance is the same.

[34] The data set used in this study mostly contains measurements made in the equinoctial seasons, with a small contribution from summer. It is known that CNA exhibits a strong seasonal variation, being greatest in the equinoctial seasons and lower in summer than in winter [*Ranta et al.*, 1983]. To a large extent, this corresponds to the long known seasonal variation in geomagnetic activity. *Russell and McPherron* [1973] proposed an explanation in terms of southward component of the interplanetary magnetic field seen by the magnetosphere as a function of the Sun–Earth geometry. More recently, it has been suggested that solar illumination of the polar regions may play an important role [*Lyatsky et al.*, 2001]. In the latter case, in particular, the seasonal variation may involve seasonal changes in the typical shape of the precipitating electron spectra [*Liou et al.*, 2001] leading to changes in the form of the CNA–conductance relationships, rather than simply affecting the occurrence probability of precipitation events. Investigation of these effects is beyond the scope of this study.

[35] It should also be borne in mind that the relationships presented in this study are derived using measurements taken in the auroral zone. At much higher or lower latitudes it is possible that the relationships would be different because of the different characteristics of particle precipitation. For example, at higher latitudes, precipitation associated with the magnetospheric cusps would occur around local noon and the precipitation associated with gradient-

**Table A2.** As for Table A1 but for the Pedersen Conductance

MLT	$c$	$m$	$p$	$A_0$	$k$	$n$	$R^2$
1900–0400	3.0 (0.52)	9.9 (0.61)	0.58 (0.069)	−0.061 (0.054)	2.1 (0.092)	11593	0.30
0400–0600	1.7 (0.49)	12 (0.89)	0.60 (0.14)	0.044 (0.075)	2.2 (0.18)	1771	0.46
0600–0800	1.1 (0.20)	6.1 (0.18)	0.54 (0.086)	0.063 (0.047)	1.4 (0.30)	2060	0.47
0800–1000	1.4 (0.38)	2.7 (0.30)	0.17 (0.091)	0.23 (0.084)	0.63 (0.11)	2880	0.40
1000–1500	1.7 (0.70)	1.2 (0.55)	0.35 (0.084)	0.20 (0.20)	0.64 (0.056)	6835	0.07

**Table A3.** As for Table A1 but for the Hall/Pedersen Conductance Ratio

MLT	$c$	$m$	$p$	$A_0$	$k$	$n$	$R^2$
1900–0400	1.4 (0.19)	1.8 (0.091)	0.56 (0.034)	0.078 (0.074)	0.12 (0.011)	11509	0.53
0400–0600	1.8 (0.22)	1.5 (0.27)	0.14 (0.091)	0.15 (0.086)	0.32 (0.032)	1688	0.51
0600–0800	2.2 (0.15)	1.7 (0.16)	0.44 (0.062)	0.084 (0.081)	0.31 (0.047)	1909	0.31
0800–1000	1.8 (0.27)	2.5 (0.24)	0.43 (0.025)	0.083 (0.032)	0.20 (0.048)	2811	0.63
1000–1500	1.2 (0.47)	2.5 (0.25)	0.63 (0.034)	−0.060 (0.13)	0.21 (0.018)	6655	0.56

curvature drift would be absent because of the open magnetic field lines.

## 5. Conclusion

[36] Statistical models for the Hall and Pedersen conductances and their ratio as functions of cosmic noise absorption at 38.2 MHz have been derived for five intervals of magnetic local time. The Hall conductance and the conductance ratio have the strongest associations with CNA and the Pedersen conductance is weakly related to CNA. The Hall conductance-CNA relationship is a strong function of MLT and this has been interpreted in terms of the change in the typical energy of precipitating electrons as they drift eastward from substorm injection. On the other hand, the conductance ratio has a relationship to CNA which is almost independent of local time. The results have been compared to the previous models of *Walker and Bhatnagar* [1989] and found to differ considerably, probably because that study did not take the MLT dependence into account. It is emphasized that the statistical nature of the models presented in this study should be borne in mind when applying them since spatially or temporally localized features in the electron precipitation will not be fully accounted for.

## Appendix A: Statistical Models

[37] In fitting the model for the mean response ( $\Sigma_H$ ,  $\Sigma_P$  or  $\Sigma_H/\Sigma_P$ ) in terms of CNA given by (6) an appropriate probability distribution for the response must be chosen. The conventional choice of a normal distribution was considered to be unsatisfactory for two reasons. First, it is unphysical since it allows negative values for parameters which can only be nonnegative, and second, for  $\Sigma_H$  and  $\Sigma_P$  in particular, it tended to produce negative values for the mean (through the constant term in (6)) at low values of CNA. Indeed, at low values of CNA the distributions of the conductances are highly asymmetric with a tail toward higher values. A potentially better candidate is the gamma distribution, which is sometimes encountered within the framework of Generalized Linear Models [*McCullagh and Nelder*, 1989]. The gamma density function is

$$f(x) = \frac{1}{\Gamma(\alpha)} \beta^{-\alpha} x^{\alpha-1} e^{-x/\beta}, \quad (\text{A1})$$

the mean is  $\mu = \alpha\beta$ , and the variance is  $\sigma^2 = \alpha\beta^2$ , where  $\alpha, \beta > 0$ .

[38] Conventionally, the response variance in a gamma model is proportional to the square of the response mean. In this data set this leads to overestimation of the variance as CNA increases. Therefore a modified gamma model with

the variance proportional to the mean  $\sigma^2 = k\mu$  was adopted (in fact,  $k = \beta$  with the parametrization of the gamma density). In some cases a constant variance might have been more appropriate. The model was fitted by maximizing the likelihood of the observed data with respect to all the model parameters, that is, the coefficients in (6) and the variance coefficient  $k$ . The maximization was constrained to avoid negative values of the coefficients in (6), except for  $A_0$ . Only data points with positive values of  $\Sigma_P$ ,  $\Sigma_H$ , or  $\Sigma_H/\Sigma_P$  were included in the fit. This excluded only a small number of points having negative values due to the subtraction of the solar ionization contribution to the conductances.

[39] Tables A1–A3 give the parameters of the fits and their estimated uncertainties (1 standard deviation). The predictive powers of the fits are measured by the  $R^2$  statistic (coefficient of determination)

$$R^2 = 1 - \frac{\sum [y_i - \mu_Y(A_i)]^2}{\sum (y_i - \bar{y})^2}, \quad (\text{A2})$$

where the subscript  $i$  ranges over each data point,  $\bar{y}$  is the mean of all response values, and  $R^2$  can be thought of as the proportion of the variance in the conductance (or ratio) which can be explained by the fit. Clearly, the closer this is to unity, the more predictive is the CNA of the conductance.

[40] When the fitting was repeated using a normal distribution, it was found that, broadly speaking, the fitted means were not greatly different. However, the detail of the fit for  $A \approx 0$  was different between the two cases, in the manner described above. On the whole it was felt that the gamma distribution gave more plausible results.

[41] **Acknowledgments.** This work was supported by grant PP/C000218/1 from the UK Particle Physics and Astronomy Research Council (PPARC). EISCAT is an international association supported by research organizations in China (CRIRP), Finland (SA), France (CNRS, until the end of 2006), Germany (DFG), Japan (NIPR and STEL), Norway (NFR), Sweden (VR), and the United Kingdom (PPARC). We are grateful to the Centre for Applied Statistics at Lancaster University for helpful comments.

[42] Wolfgang Baumjohann thanks Stephen Buchert and Johan Stadsnes for their assistance in evaluating this paper.

## References

- Aksnes, A., J. Stadsnes, N. Østgaard, G. A. Germany, K. Oksavik, R. R. Vondrak, A. Brekke, and U. P. Løvhaug (2006), Height profiles of the ionospheric electron density derived using space-based remote sensing of UV and X ray emissions and EISCAT radar data: A ground-truth experiment, *J. Geophys. Res.*, *111*, A02301, doi:10.1029/2005JA011331.
- Ashrafi, M., M. J. Kosch, and F. Honary (2005), Comparison of the characteristic energy of precipitating electrons derived from ground-based and DMSP satellite data, *Ann. Geophys.*, *23*, 135–145.
- Baker, D. N., P. Stauning, E. W. Hones Jr., P. R. Higbie, and R. D. Belian (1981), Near-equatorial, high-resolution measurements of electron precipitation at  $L \simeq 6.6$ , *J. Geophys. Res.*, *86*, 2295–2313.

- Bewersdorff, A., J. Dion, G. Kremser, E. Keppler, J. P. Legrand, and W. Riedler (1966), Diurnal energy variation of auroral X-rays, *Ann. Geophys.*, *22*, 23–30.
- Brekke, A., and C. Hall (1988), Auroral ionospheric quiet summer time conductances, *Ann. Geophys.*, *6*, 361–376.
- Brekke, A., C. Hall, and T. L. Hansen (1989), Auroral ionospheric conductances during disturbed conditions, *Ann. Geophys.*, *7*, 269–280.
- Brown, R. R. (1966), Electron precipitation in the auroral zone, *Space Sci. Rev.*, *5*, 311–387.
- Browne, S., J. K. Hargreaves, and B. Honary (1995), An imaging riometer for ionospheric studies, *Electron. Commun. Eng. J.*, *7*, 209–217.
- Collis, P. N., J. K. Hargreaves, and A. Korth (1984), Auroral radio absorption as an indicator of magnetospheric electrons and of conditions in the disturbed auroral D region, *J. Atmos. Terr. Phys.*, *46*, 21–38.
- Davies, J. A., and M. Lester (1999), The relationship between electric fields, conductances, and currents in the high-latitude ionosphere: A statistical study using EISCAT data, *Ann. Geophys.*, *17*, 43–52.
- Davies, J. A., and T. R. Robinson (1997), Heating of the high-latitude ionospheric plasma by electric fields, *Adv. Space Res.*, *20*, 1125–1128.
- Detrick, D. L., and T. J. Rosenberg (1990), A phased-array radiowave imager for studies of cosmic noise absorption, *Radio Sci.*, *25*, 325–338.
- Hardy, D. A., M. S. Gussenhoven, and E. Holeman (1985), A statistical model of auroral electron precipitation, *J. Geophys. Res.*, *90*, 4229–4248.
- Hargreaves, J. K. (1968), Auroral motions observed with riometers: latitudinal movements and a median global pattern, *J. Atmos. Terr. Phys.*, *30*, 1461–1470.
- Hargreaves, J. K. (1969), Auroral absorption of HF radio waves in the ionosphere: A review of results from the first decade of riometry, *Proc. IEEE*, *57*, 1348–1373.
- Hargreaves, J. K., and T. Devlin (1990), Morning sector electron precipitation events observed by incoherent scatter radar, *J. Atmos. Terr. Phys.*, *52*, 193–203.
- Janhunen, P. (2001), Reconstruction of electron precipitation characteristics from a set of multiwavelength digital all-sky auroral images, *J. Geophys. Res.*, *106*, 18,505–18,516.
- Jelly, D., and N. Brice (1967), Changes in Van Allen radiation associated with polar substorms, *J. Geophys. Res.*, *72*, 5919–5931.
- Kavanagh, A. J., M. J. Kosch, F. Honary, A. Senior, S. R. Marple, E. E. Woodfield, and I. W. McCrea (2004), The statistical dependence of auroral absorption on geomagnetic and solar wind parameters, *Ann. Geophys.*, *22*, 877–887.
- Kodama, M., H. Suzuki, Y. Hirasima, T. Yamagami, H. Murakami, and J. Nishimura (1995), Circumpolar observation of bremsstrahlung X-rays by a polar patrol balloon over Antarctica, *J. Geomag. Geoelectr.*, *47*, 253–266.
- Kosch, M. J., T. Hagfors, and K. Schlegel (1998), Extrapolating EISCAT Pedersen conductances to other parts of the sky using ground-based TV auroral images, *Ann. Geophys.*, *16*, 583–588.
- Kosch, M. J., F. Honary, C. F. del Pozo, S. R. Marple, and T. Hagfors (2001), High-resolution maps of the characteristic energy of precipitating auroral particles, *J. Geophys. Res.*, *106*, 28,925–28,937.
- Lehtinen, M. S., and A. Huuskonen (1996), General incoherent scatter analysis and GUISDAP, *J. Atmos. Terr. Phys.*, *58*, 435–452.
- Liou, K., P. T. Newell, and C.-I. Meng (2001), Seasonal effects on auroral particle acceleration and precipitation, *J. Geophys. Res.*, *106*, 5531–5542.
- Lyatsky, W., P. T. Newell, and A. Hamaza (2001), Solar illumination as cause of the equinoctial preference for geomagnetic activity, *Geophys. Res. Lett.*, *28*, 2353–2356.
- Makarevitch, R. A., F. Honary, I. W. McCrea, and V. S. C. Howells (2004), Imaging riometer observations of drifting absorption patches in the morning sector, *Ann. Geophys.*, *22*, 3461–3478.
- McCullagh, P., and J. A. Nelder (1989), *Generalized Linear Models*, 2nd ed., Chapman and Hall, London.
- Mori, H., M. Ishii, Y. Murayama, M. Kubota, K. Sakanoi, M.-Y. Yamamoto, Y. Monzen, D. Lummerzheim, and B. J. Watkins (2004), Energy distribution of precipitating electrons estimated from optical and cosmic noise absorption measurements, *Ann. Geophys.*, *22*, 1613–1622.
- Partamies, N., P. Janhunen, K. Kauristie, S. Mäkinen, and T. Sergienko (2004), Testing an inversion method for estimating electron energy fluxes from all-sky camera images, *Ann. Geophys.*, *22*, 1961–1971.
- Ranta, H., A. Ranta, T. J. Rosenberg, and D. L. Detrick (1983), Autumn and winter anomalies in ionospheric absorption as measured by riometers, *J. Atmos. Terr. Phys.*, *45*, 193–202.
- Rees, M. H. (1963), Auroral ionization and excitation by incident energetic electrons, *Planet. Space Sci.*, *11*, 1209–1218.
- Rishbeth, H., and A. P. van Eyken (1993), EISCAT: Early history and the first ten years of operation, *J. Atmos. Terr. Phys.*, *55*, 525–542.
- Robinson, R. M., R. R. Vondrak, K. Miller, T. Dabbs, and D. Hardy (1987), On calculating ionospheric conductances from the flux and energy of precipitating electrons, *J. Geophys. Res.*, *92*, 2565–2569.
- Roederer, J. G. (1967), On the adiabatic motion of energetic particles in a model magnetosphere, *J. Geophys. Res.*, *72*, 981–992.
- Russell, C. T., and R. L. McPherron (1973), Semiannual variation of geomagnetic activity, *J. Geophys. Res.*, *78*, 92–108.
- Schunk, R. W., and A. F. Nagy (1978), Electron temperatures in the F region of the ionosphere: Theory and observations, *Rev. Geophys. Space Phys.*, *16*, 355–399.
- Schunk, R. W., and J. C. G. Walker (1973), Theoretical ion densities in the lower ionosphere, *Planet. Space Sci.*, *21*, 1875–1896.
- Stauning, P. (1984), Absorption of cosmic noise in the E region during electron heating events: A new class of riometer absorption events, *Geophys. Res. Lett.*, *11*, 1184–1187.
- Thomsen, M. F., J. Birn, J. E. Borovsky, K. Morzinski, D. J. McComas, and G. D. Reeves (2001), Two-satellite observations of substorm injections at geosynchronous orbit, *J. Geophys. Res.*, *106*, 8405–8416.
- Vickrey, J. F., R. R. Vondrak, and S. J. Matthews (1981), The diurnal and latitudinal variation of auroral zone ionospheric conductivity, *J. Geophys. Res.*, *86*, 65–75.
- Walker, J. K., and V. P. Bhatnagar (1989), Ionospheric absorption, typical ionization, conductivity, and possible synoptic heating parameters in the upper atmosphere, *J. Geophys. Res.*, *94*, 3713–3720.

---

F. Honary, A. J. Kavanagh, M. J. Kosch, and A. Senior, Department of Communication Systems, Lancaster University, Lancaster LA1 4WA, UK. (a.senior@lancaster.ac.uk)